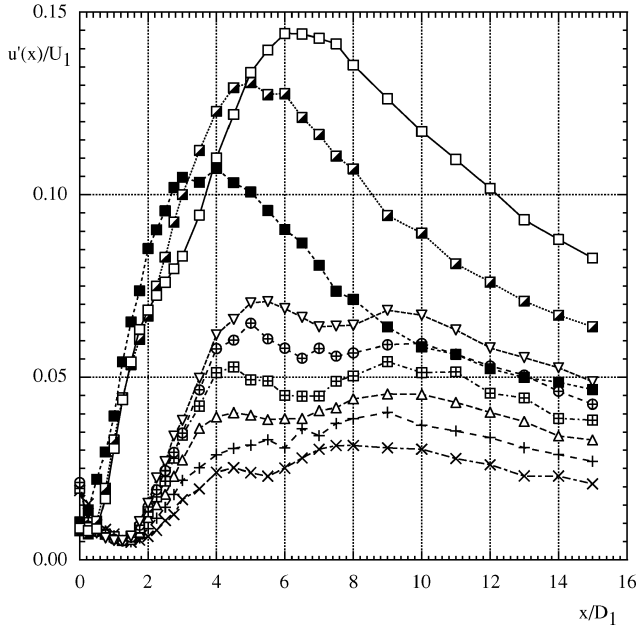

a)

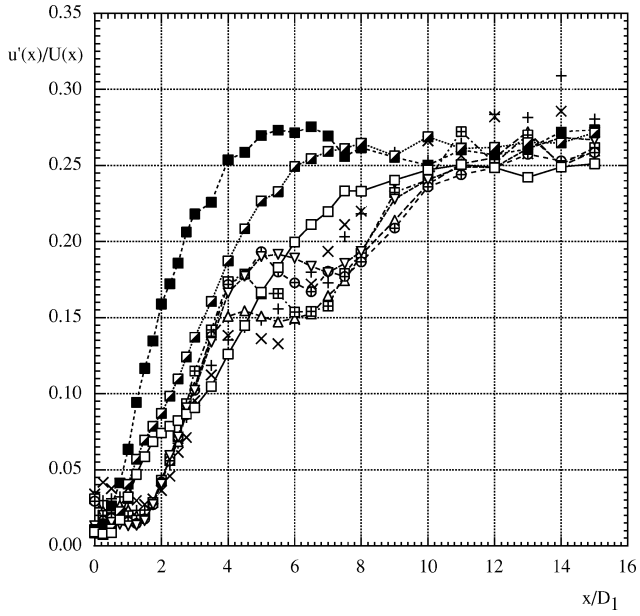

b)

Fig. 5 Axial profiles: a) turbulent velocity fluctuation rms and b) turbulent intensity. Symbols are the same as in Fig. 2.

Conclusions

The present results clearly show the existence of two regimes in the diffusion of jets with annular counterflow and small diameter ratio. For $R \leq 0.2$, the combination of a high level of suction and a narrow slot gives rise to a strong enhancement of the jet diffusion and turbulent activity. However, it has been shown[3] that a fraction of the central flow rate is ingested into the slot for a tube jet and the same diameter ratio. Furthermore, this fraction grows with R. It is likely that the same phenomenon occurs with the present nozzle. This probably contributes to increase the spreading of the central jet and to accelerate the decrease of $U(x)$ inside the collar (Fig. 2). For $R \geq 0.28$, the central jet completely fills the collar exit section and effect of the suction is simply to give birth to a standard jet of reduced initial mass flow rate and increased diameter. It is clear that this second regime is of minor interest for practical applications.

Acknowledgment

The authors acknowledge the region Rhône-Alpes for supporting the visit of D. Asendrych in Grenoble.

References

[1]Strykowski, P., and Wilcoxon, R. K., "Mixing Enhancement Due to Global Oscillations in Jets with Annular Counterflow," *AIAA Journal*, Vol. 31, No. 3, 1993, pp. 564–570.

[2]Boguslawski, A., Favre-Marinet, M., and Abdulwahab, A., "Contrôle des Jets par Écoulement à Contre-Courant," *Comptes Rendus de l'Académie des Sciences, Série IIb*, Vol. 327, 1999, pp. 589–595.

[3]Favre-Marinet, M., and Boguslawski, A., "Jet Control by Counterflow," *Turbulence and Shear Flow Phenomena 1*, edited by S. Banerjee and J. K. Eaton, Begell House, New York, 1999, pp. 659–664.

[4]Lourenco, L., Shen, H., Krothapalli, A., and Strykowski, P., "Whole-Field Measurements on an Excited Premixed Flame Using On-Line PIV," *8th International Symposium on Applications of Laser Techniques to Fluid Mechanics*, Springer-Verlag, Berlin, 1996, pp. 425–437.

[5]Chan, S. M. S., Torii, S., and Yano, T., "Enhancement of Turbulent Jet Diffusion Flame Blowout Limits by Annular Counterflow," *International Journal of Energy Research*, Vol. 25, No. 12, 2001, pp. 1091–1105.

[6]Asendrych, D., and Drobniak, S., "Experimental Analysis of the Flowfield in Non-Isothermal Countercurrent Jets," *Advances in Turbulence IX*, edited by I. P. Castro, P. E. Hancock, and T. G. Thomas, CIMNE, Barcelona, 2002, p. 839.

S. Aggarwal
Associate Editor

Boundary-Layer Loss Mechanism and Assessment of Wall Functions for Turbulence Modeling

Ge-Cheng Zha*
University of Miami, Coral Gables, Florida 33124

I. Introduction

As Denton pointed out in his well-known paper "Loss Mechanisms in Turbomachines,"[1] the measure of performance for internal flows is the energy loss, which is directly related to the efficiency of a machine. The entropy is usually used to measure the loss. Denton derived the total rate of entropy creation across an adiabatic boundary layer as the following:

$$\dot{S}_a = \frac{\mathrm{d}}{\mathrm{d}x}\int_0^\delta [\rho V_x(s - s_\delta)]\,\mathrm{d}y = \int_0^\delta \frac{1}{T}\tau_{xy}\,\mathrm{d}V_x \qquad (1)$$

Denton hence concluded that the shear-stress work is the sole source for the entropy creation of an adiabatic boundary layer. Denton further extended the conclusion of Eq. (1) to the local rate of entropy creation within a boundary layer as

$$\dot{S}_v = \frac{1}{T}\tau\frac{\mathrm{d}V}{\mathrm{d}y} \qquad (2)$$

Based on the shear-stress work distribution within a boundary layer, Denton indicated that most of the entropy creation is within

Presented as Paper 2004-1118 at the AIAA 42nd Aerospace Sciences Meeting, Reno, NV, 5–8 January 2004; received 3 March 2004; revision received 28 July 2004; accepted for publication 28 July 2004.

*Associate Professor, Department of Mechanical Engineering; zha@apollo.eng.miami.edu. Member AIAA.

the viscous sublayer and the logarithmic region. Denton also referred to Dawes's results,[2] which shows that 90% of the entropy generation occurs within the inner part of a turbulent boundary layer. The inner layer is a very thin layer from the solid wall surface to the logarithmic layer (2 to 20% of the boundary-layer thickness[3]) compared with the overall thickness of a turbulent boundary layer.

If the preceding conclusions were true, we then face a serious challenge: the widely used wall-function boundary conditions would be incorrect to predict the flow loss. The concept of wall functions is to use the law of the wall to save CPU time by avoiding resolving the inner layer of a turbulent boundary layer when the transport equations of the turbulence are solved.[4] The wall-function concept is used for both Reynolds-averaged Navier–Stokes and large-eddy-simulation flow solvers. The first grid point is usually located in the logarithmic layer, that is, $30 \leq y^+ \leq 150$. However, inferring from Denton's theory,[1] we can conclude that wall-function methods, which ignore the inner layer where most of the entropy is created, would significantly underpredict the loss and could not be used for internal flows.[5] This seems contradictory to the common practice to use wall functions to simulate the internal flows.

Obviously, the boundary-layer energy loss mechanism is not well understood, and using wall function to predict the flow energy loss is not assessed even though the wall-function method is widely used.

The objectives of this Note are twofold: 1) study the loss mechanism for an adiabatic boundary layer, and 2) examine the applicability of wall function for internal flow loss prediction.

II. Boundary-Layer Loss Mechanism

To study the boundary-layer loss mechanism, we will begin with the steady-state boundary-layer equations[3] for a flat plate, which include the continuity equation, x- and y-momentum equations, and the energy equation. In Ref. 4, a detailed derivation is given, and the following local entropy creation rate along a infinitesimally thin streamtube is obtained:

$$\frac{\partial s}{\partial l}\,\mathrm{d}\dot{m} = \frac{1}{T}\left(\tau_{xy}\frac{\partial u}{\partial y}\,\mathrm{d}y - \frac{\partial q}{\partial y}\,\mathrm{d}y\right) \tag{3}$$

or

$$\frac{\partial s}{\partial l}\,\mathrm{d}\dot{m} = \frac{1}{T}(\tau_{xy}\,\mathrm{d}u - \mathrm{d}q) \tag{4}$$

where $\mathrm{d}\dot{m}$ is the mass flow rate in the infinitesimally thin streamtube.

Equation (4) indicates that the local entropy creation rate along a streamtube within a boundary layer is caused by the shear-stress work and heat-flux variation. Even for the adiabatic boundary layer of incompressible flow, the temperature variation is small, but the $\mathrm{d}q$ or $\mathrm{d}q/\mathrm{d}y$ are large and have the same order of magnitude as the shear-stress work. This is demonstrated by the theoretical analysis[3] and the numerical results presented in the next section of this Note.

The total rate of the entropy creation $\dot{S}_a$ can be obtained by integrating Eq. (3) or (4), that is,

$$\dot{S}_a = \int_0^{\dot{m}_\delta} \frac{\partial s}{\partial l}\,\mathrm{d}\dot{m} = \int_0^{\delta} \frac{1}{T}\left(\tau_{xy}\frac{\partial u}{\partial y} - \frac{\partial q}{\partial y}\right)\mathrm{d}y \tag{5}$$

or

$$\dot{S}_a = \int_0^{\dot{m}_\delta} \frac{\partial s}{\partial l}\,\mathrm{d}\dot{m} = \int_0^{\delta} \frac{1}{T}(\tau_{xy}\,\mathrm{d}u - \mathrm{d}q) \tag{6}$$

where $\dot{m}_\delta$ stands for the total mass flow across the boundary layer.

When wall functions are used, the preceding formulations become

$$\dot{S}_a = \int_{\dot{m}_{\text{wall function}}}^{\dot{m}_\delta} \frac{\partial s}{\partial l}\,\mathrm{d}\dot{m} = \int_{y_{\text{wall function}}}^{\delta} \frac{1}{T}(\tau_{xy}\,\mathrm{d}u - \mathrm{d}q) \tag{7}$$

For an adiabatic boundary layer, the temperature usually does not vary as largely as the shear-stress work and heat flux. In the preceding integrals, it is reasonable to treat the temperature as a constant. Using the boundary conditions that $q = 0$ on the wall surface and at the edge of the boundary layer, Eq. (6) becomes

$$\dot{S}_a = \int_0^{\dot{m}_\delta} \frac{\partial s}{\partial l}\,\mathrm{d}\dot{m} = \int_0^{\delta} \frac{1}{T}\tau_{xy}\,\mathrm{d}u \tag{8}$$

This means that the total rate of entropy creation across a boundary layer is equal to the total shear-stress work in the boundary layer, which is the same as Denton's conclusion [Eq. (1)]. However, simply extending Eq. (8) to determine the local rate of entropy creation as Eq. (2) is incorrect. The local rate of entropy creation is determined by Eq. (3) or (4). The $\mathrm{d}q$ in Eq. (4), or $(\partial q/\partial y)\,\mathrm{d}y$ in Eq. (3), has a very important contribution to the local entropy creation. It is just canceled out after doing the integral across the boundary layer.

In other words, when we say that the total rate of entropy creation across a boundary layer is equal to the shear-stress work it is only correct in the quantitative sense. It is misleading to think it actually occurs that way. Physically, both heat-flux variation and shear-stress work cause entropy creation. These two factors always coexist and interact each other everywhere in the whole boundary layer.

III. Quantitative Analysis of Entropy Creation

An ideal-gas turbulent boundary layer in an adiabatic channel is solved numerically using Fluent computational-fluid-dynamics solver to obtain the database for analysis. The total pressure, temperature, and 0-deg flow angle at the inlet and a static pressure at the exit are specified. The exit static pressure is adjusted to match the inlet Mach number of 0.2 so that the flow is in the incompressible regime, which will facilitate the validation of the numerical solutions. The duct has an aspect ratio of 25. The Reynolds number based on the duct height is $Re_h = 10^5$. The two equation k–ϵ model is used with the low-Reynolds-number model integrating to the wall, which is a two-layer model based on the blending method suggested by Jongen.[6] The near-wall turbulence viscosity is obtained by using the one-equation model of Wolfstein.[7] A second-order accuracy differencing scheme is used. The no-slip adiabatic boundary conditions are imposed on the solid wall. The mesh size is 101×81. The y^+ for the first grid adjacent to the wall is $y_1^+ = 1.8$.

Even though we want to study the entropy creation predicted by using the wall functions, the benchmark solution needs to be integrated to the wall so that the whole boundary-layer profile can be obtained. The solutions with wall-function boundary conditions are a subset of the solution integrated to the wall. Hence the evaluation of using the wall functions will be still based on the results from the solution integrated to the wall.

The numerical solution is fully validated in Ref. 4. The velocity and temperature profiles agree excellently with the law of wall and Crocco–Busemann formulation.[3] The computed dissipation coefficient also agrees accurately with the results from the correlation given in Ref. 8. The mesh-refinement study indicated that the solution is mesh-size independent. The numerical solution is hence sufficiently accurate to provide the database for further entropy creation analysis.

Figure 1 is the shear-stress distribution vs velocity across the boundary layer. According to Eqs. (1) and (8), the total area under the curve is the total rate of entropy creation across the boundary layer. As pointed out by Denton,[1] most of the shear-stress work occurs in the inner layer. For the present case at $y^+ = 30$, it takes about 62% of the total area. For $y^+ = 107$, it is 78% of the area. Obviously, inferred from Denton's theory, the wall functions located in the logarithmic layer with $30 \leq y^+ \leq 150$ will miss most of the entropy creation, or the loss prediction.

Now, let us examine the contribution of the local entropy creation from the two terms of Eq. (3) and their resultant as shown in Fig. 2. The dashed line is $\tau_{xy}\,\mathrm{d}u/\mathrm{d}y$ vs y^+. Figure 3 shows the zoomed part of Fig. 2 near the wall. $\tau_{xy}\,\mathrm{d}u/\mathrm{d}y$ has a very large value near the

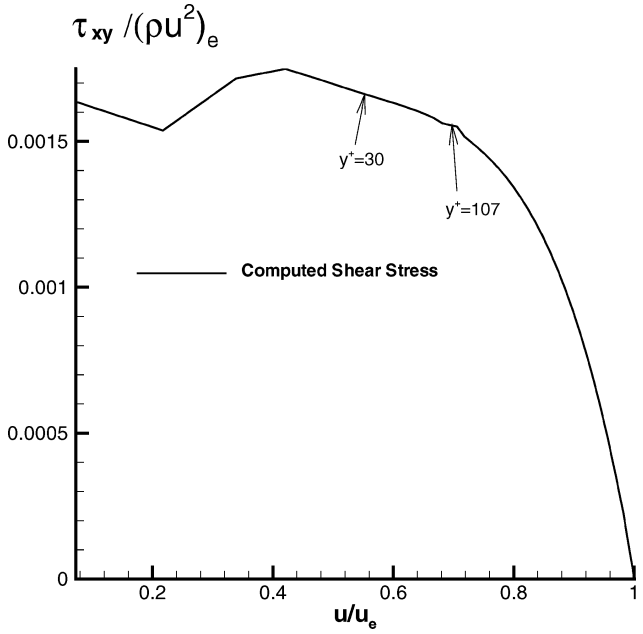

Fig. 1 Distribution of entropy creation caused by shear-stress work across the boundary layer.

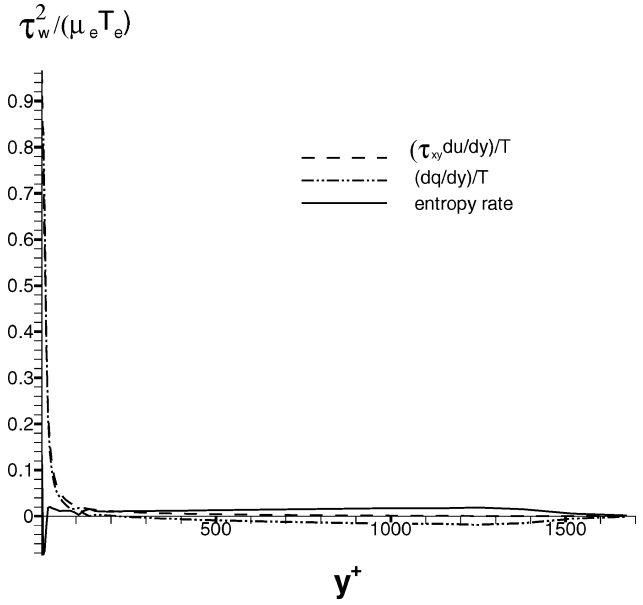

Fig. 2 Distribution of entropy creation across the boundary layer for individual terms and their resultant.

wall because of the large velocity gradient. This again shows that the near-wall region takes most of the area under the dashed line as indicated in Fig. 1.

However, the heat-flux gradient near the wall is also very large and is in the same order of magnitude as the shear-stress work. The large rate of entropy creation caused by $\tau_{xy}\,\mathrm{d}u/\mathrm{d}y$ is offset by the heat-flux gradient. On the wall surface, the $\tau_{xy}\,\mathrm{d}u/\mathrm{d}y$ is greater than the $\mathrm{d}q/\mathrm{d}y$ and results in the maximum entropy creation rate on the wall surface (see Fig. 3). Above the viscous sublayer, the $\mathrm{d}q/\mathrm{d}y$ increases more rapidly than the $\tau_{xy}\,\mathrm{d}u/\mathrm{d}y$ and creates a local negative valley of the rate of entropy creation very close to the wall with the y^+ from about 5 to 20 (the solid line).

The solid line in Fig. 2 shows that the resultant local rate of entropy creation [Eq. (3)] is fairly uniform for most part of the boundary layer except near the wall and gradually reduces to zero at the edge of the boundary layer. Through the whole boundary layer,

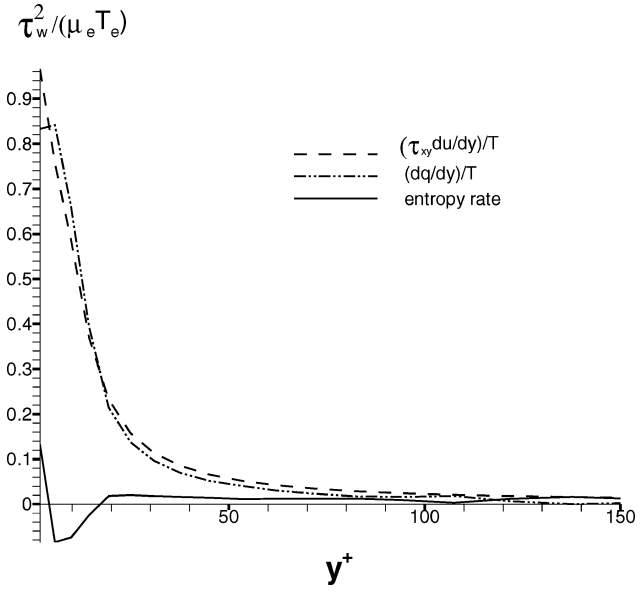

Fig. 3 Distribution of entropy creation near the wall for individual terms and their resultant.

the $\tau_{xy}\,\mathrm{d}u/\mathrm{d}y$ and $\mathrm{d}q/\mathrm{d}y$ have the same order of magnitude. The integral of the total rate of entropy creation is the area under the solid line according to Eq. (5). This area is equal to area of Fig. 1 quantitatively. It is also equal to the area under the dashed line in the same plot of Fig. 2.

With the preceding analysis, we can examine the effect of using wall functions on the total rate of entropy creation rate. To clearly see the contribution of each term, the integrals of shear-stress work and heat-flux gradient of Eq. (5) are separated as follows:

$$\dot{S}_a = \int_{\dot{m}_{\text{wall function}}}^{\dot{m}_\delta} \frac{\partial s}{\partial l}\,\mathrm{d}\dot{m} = \int_{y_{\text{wall function}}}^{\delta} \frac{1}{T}\tau_{xy}\frac{\partial u}{\partial y}\,\mathrm{d}y - \int_{y_{\text{wall function}}}^{\delta} \frac{1}{T}\frac{\partial q}{\partial y}\,\mathrm{d}y \tag{9}$$

Equation (9) can be normalized by $\rho_e u_e^3/T_e$. That is,

$$\dot{S}_a = Cd - Ch \tag{10}$$

where

$$Cd = \frac{T_e}{\rho_e u_e^3}\int_{y_{\text{wall function}}}^{\delta} \frac{1}{T}\tau_{xy}\frac{\partial u}{\partial y}\,\mathrm{d}y \tag{11}$$

$$Ch = \frac{T_e}{\rho_e u_e^3}\int_{y_{\text{wall function}}}^{\delta} \frac{1}{T}\frac{\partial q}{\partial y}\,\mathrm{d}y \tag{12}$$

Cd is defined as the dissipation coefficient.[8] Ch is the heat-transfer coefficient. Obviously, Cd, Ch, and $\dot{S}_a$ will vary with the location of the $y_{\text{wall function}}$. Figure 4 shows such variations. For comparison purposes, the dash-dot-dot line is the benchmark total rate of entropy creation integrated from the wall surface as defined in Eq. (5).

When integrated from the wall surface, as explained for Eq. (8), the following results are expected:

$$\dot{S}_a \approx Cd, \qquad Ch \approx 0 \tag{13}$$

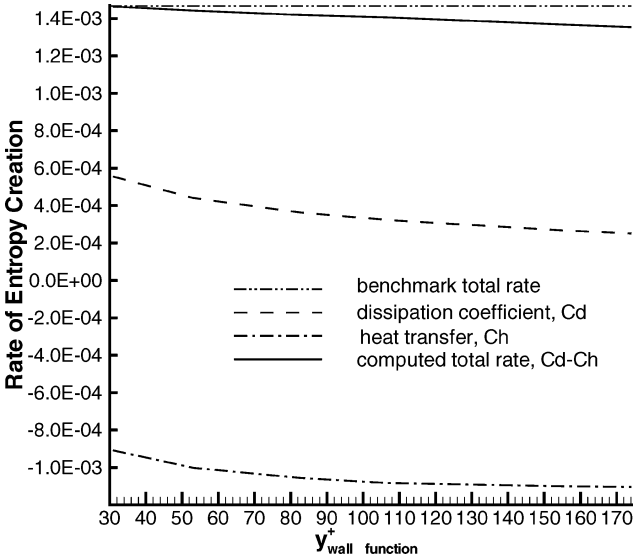

Fig. 4 Entropy creation rate computed at different wall-function location.

The following are the values obtained from the numerical results:

$$Cd = 0.00146343, \qquad Ch = -0.00000553$$

$$\dot{S}_a = Cd - Ch = 0.00146896 \tag{14}$$

The value of Cd agrees excellently with the value of 0.001432 calculated by the correlation given in Refs. 4 and 8. The Ch is indeed nearly zero. This again indicates that the numerical results are accurate.

The $y_{\text{wall function}}$ needs to be located in the logarithmic layer and is usually in the range of $y^+ = 30$–150. Figure 4 shows that when $y^+_{\text{wall function}}$ varies from 30 to 170, Cd alone is significantly lower than the benchmark total rate of the entropy creation. When the contribution of Ch is added, the computed total rate of entropy creation using wall functions, the solid line, is very close to the benchmark solution. In particular, if the $y^+_{\text{wall function}}$ has the low value such as 30 the difference of the computed total rate of entropy creation from the benchmark solution is negligible. The contribution from Ch is about twice larger than the shear-stress work Cd at $y^+_{\text{wall function}} = 30$ and five times larger at $y^+_{\text{wall function}} = 150$.

If only the shear-stress work were considered as the total rate of entropy creation as given in Eq. (2) by Denton, the error would be from 62 to 82% when the $y^+_{\text{wall function}}$ varies from 30 to 170. When the heat-flux gradient is added, the error is dramatically reduced to 0.34 to 7.8%. For loss prediction in engineering application, this error range is within the prediction uncertainty and might be acceptable. In particular, if the wall functions are used at y^+ about 30, the difference of the loss prediction between using wall functions and integrating to the wall is negligible.

A case of compressible flow with Mach number of 0.95 for the duct shows the same behavior as the incompressible case, both qualitatively and quantitatively. To save space, the results of the Mach 0.95 case are not shown here.

In Ref. 4, the numerical solutions of a transonic cascade using wall functions and integrating to the wall are compared. The wake profiles of the two solutions agree very well. The difference of the loss prediction using the two methods is 0.8%, which is small and is consistent with the error range given from the loss mechanism theory of this Note.

The negative values observed near the wall in Figs. 2 and 3 derive from the fact that the quantity plotted is proportional to the substantial derivative of entropy and depend not only on the nonnegative local generation process but also diffusion through molecular processes as a result of the heat transfer. Thus, although the integral over the boundary layer yields net entropy increase as required from the second law there are local regions where entropy change is negative. Indeed, the computed entropy creation rate, the velocity profiles, and the temperature profiles agree with those determined from Schlichting[4,8] and the Crocco–Busemann formulation.[3,4]

IV. Conclusions

The mechanism of entropy creation in an adiabatic boundary layer is studied. The local entropy creation rate has two sources: shear-stress work and heat-flux gradient. These two factors have the same order of magnitude everywhere in the boundary layer. Their balance results in a fairly uniform distribution of entropy creation rate across the boundary layer. In the inner-layer region, the large rate of entropy creation as a result of the velocity gradient and shear stress is offset by the gradient of the heat flux. A negative entropy change rate area near the wall is observed caused by the local heat transfer.

With the new understanding of the entropy creation mechanism, this study justifies that the wall function methods are applicable to internal flow loss prediction. For a Mach 0.2 adiabatic boundary layer in a two-dimensional channel with no separation, the error of the total rate of entropy creation varies from 0.34 to 7.8% when the wall functions are applied at $y^+ = 30$–170. This error is within the engineering application uncertainty. The compressible flow case of Mach 0.95 shows the same behavior as the incompressible case.

The previous theory of local entropy creation in a boundary layer given by Denton did not include the heat-flux gradient factor. The sole contribution to the local entropy creation rate was considered as the shear-stress work. Using Denton's theory to study the applicability of wall-function methods for internal flow loss prediction would lead to a very large unacceptable error in the range of 60 to 80%. According to the study in this Note, such a large error is false and is caused by ignoring the heat-flux gradient contribution to the local rate of entropy creation.

Acknowledgments

The General Research Support Award from the University of Miami to support this research is acknowledged. This Note originated from the author's course project at the Massachusetts Institute of Technology (MIT).[5] The author thanks E. Greitzer at MIT for his encouragement to pursue this work.

References

[1]Denton, J., "Loss Mechanisms in Turbomachines," *Journal of Turbomachinery*, Vol. 115, Oct. 1993, pp. 621–656.

[2]Dawes, W., "A Comparison of Zero and One Equation Turbulence Modeling for Turbomachinery Calculations," American Society of Mechanical Engineers, Paper 90-GT-303, June 1990.

[3]White, F. M., *Viscous Fluid Flow*, 2nd ed., McGraw–Hill, New York, 1991, Chap. 7.

[4]Zha, G.-C., "Boundary Layer Loss Mechanism and Justification of Wall Functions for Turbulence Modeling," AIAA Paper 2004-1118, Jan. 2004.

[5]Zha, G.-C., "The Defect of Computing Losses Using Wall Functions for Turbulent Internal Flows," Massachusetts Inst. of Technology, Project Rept. No. 2, Course 16.51, Internal Flows, Cambridge, MA, 28 March 2000.

[6]Jongen, T., "Simulation and Modeling of Turbulent Incompressible Flows," Ph.D. Dissertation, EPF, Lausanne, Switzerland, 1992.

[7]Wolfstein, M., "The Velocity and Temperature Distribution of One-Dimensional Flow with Turbulence Augmentation and Pressure Gradient," *Journal of Heat and Mass Transfer*, Vol. 12, 1969, pp. 301–318.

[8]Schlichting, H., *Boundary Layer Theory*, 7th ed., McGraw–Hill, New York, 1979.

D. Gaitonde
Associate Editor